Sliding conductivity of a magnetic kink crystal in a chiral helimagnet

Jun-ichiro Kishine
Department of Basic Sciences, Kyushu Institute of Technology, Kitakyushu 804-8550, Japan

A. S. Ovchinnikov and I. V. Proskurin
Department of Physics, Ural State University, Ekaterinburg 620083, Russia

(Received 1 May 2010; revised manuscript received 15 July 2010; published 6 August 2010)

We derive a current-driven sliding conductivity of the magnetic kink crystal (MKC) in chiral helimagnet under weak magnetic field applied perpendicular to the helical axis. For this purpose, we discuss the correlated dynamics of quantum-mechanical itinerant spins and the MKC which are coupled via the sd exchange interaction. The itinerant spins are treated as fully quantum-mechanical operators whereas the dynamics of the MKC is considered within classical Lagrangian formalism. By appropriately treating elementary excitations around the MKC state, we construct coupled equations of motion for the collective coordinates (the center-of-mass position and quasi-zero-mode coordinate) associated with the sliding motion of the MKC. By solving them, we demonstrate that the correlated dynamics is understood through a hierarchy of two time scales: Boltzmann relaxation time τ_{el}, when a nonadiabatic spin-transfer torque appears, and Gilbert damping time τ_{MKC}, when adiabatic spin-transfer torque comes up. As a notable consequence, we found that the terminal velocity of the sliding motion reverses its sign depending on the band-filling ratio of the conduction electron system.

DOI: 10.1103/PhysRevB.82.064407 PACS number(s): 75.30.−m, 75.47.−m, 85.75.Ss

I. INTRODUCTION

Spin textures coupled to spin-polarized electric current have attracted considerable interest from both theoretical and experimental viewpoints. For example, current-driven domain-wall (DW) motion in a ferromagnet by using spin-polarized current is a main issue in far-reaching field of spintronics.[1–3] From fundamental viewpoints, the main interest lies in nontrivial interference of quantum and semiclassical dynamics, i.e., linear Hamiltonian dynamics in quantum system couples with nonlinear dissipative dynamics in classical system. Recent theoretical studies[4–12] have disclosed mechanisms of spin-transfer-torque (STT) processes in the current-driven domain-wall motion. According to these works, the STT consists of two parts, i.e., adiabatic STT, $\mathcal{T}_1$,[1,6] and nonadiabatic STT, $\mathcal{T}_2$.[10] The origin of $\mathcal{T}_1$ is understood based on the Döring-Becker-Kittel mechanism of the domain-wall motion in ferromagnets,[13] where the moving DW accompanies the internal deformation and causes the spontaneous demagnetization field. On the other hand, the terminal velocity of a DW is controlled by $\mathcal{T}_2$ whose origin is ascribed to the spatial mistracking between conduction electrons' spin and local magnetization.[10] Behind appearance of the $\mathcal{T}_2$ term is the so-called transverse spin accumulation (TSA) of itinerant electrons generated by the electric current.[5,11] TSA means the effect where the component of electron spin vector perpendicular to the local moment acquires finite expectation value.

It is now a natural step to survey wider classes of topological spin textures other than the domain walls. Actually, there have emerged interests in the current-driven magnetization dynamics of complex topological spin textures, such as spin vortex walls,[14] spiral spin texture,[11] helical spin-density waves,[15,16] and skyrmion lattice.[17] One of the best candidate along this line is a chiral helimagnet. Chiral helimagnetic state is characterized by the vector spin chirality as an order parameter. The structure is stabilized by the antisymmetric Dzyaloshinskii-Moriya (DM) interaction[18] and realized in crystals without rotoinversion symmetry. Chirality means that either left-handed or right-handed incommensurate helical spin modulation is selected by the direction of the DM vector. In the context of Landau theory of phase transitions, the existence of the Lifshitz invariant in the free energy justifies the chiral helimagnetic order.[19] As shown in Fig. 1(a), under the magnetic field applied perpendicular to the helical axis, the ground state possesses a periodic array of the commensurate (C) and incommensurate (IC) domains partitioned by discommensurations, i.e., the *internal lattice* which is called magnetic kink crystal (MKC) or sometimes referred to as chiral soliton lattice[19,20] is stabilized. As the magnetic field strength increases, the spatial period of MKC lattice, L_{kink}, increases and finally goes to infinity at the critical field strength. In this case, the ground state has infinite

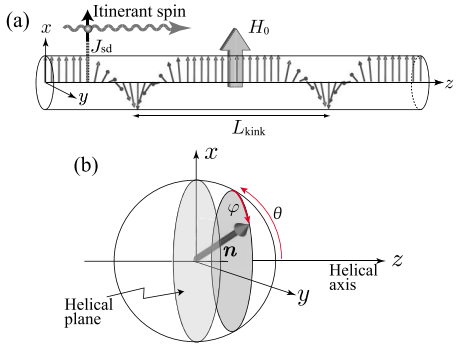

FIG. 1. (Color online) (a) MKC state coupled with itinerant spins via the sd coupling. The magnetic field strength must satisfy the weak field condition ($\omega_c \tau_{\mathrm{el}} \ll 1$) discussed in Sec. IV, where ω_c is the cyclotron resonance frequency and τ_{el} is the Boltzmann relaxation time of conduction electrons. (b) The polar coordinates used here.

degeneracy associated with arbitrary choice of the center-of-mass position. Consequently, the *translational* symmetry along the helical axis is spontaneously broken. Present authors have discussed physical outcome of the MKC state from various view points.[21–23]

From more fundamental viewpoints, the chiral helimagnet sheds light on two basic notions in condensed-matter physics, i.e., macroscopic manifestations of the quantum phase and physical outcome of chirality.[24] Both notions have been separately taken up in various contexts. For example, the Josephson effect in superconductors and the collective charge-/spin-density-wave transport in quasi-one-dimensional (Q1D) systems are typical issue related to the former subject. The notion of chiralty has more interdisciplinary meaning which covers from geometrical chirality of molecular structure to spin chirality in frustrated magnets. However, to directly observe any physical quantity related to the phase and chirality is not easy, because it is quite nontrivial to seek for physical field which directly couple with these degrees of freedom.

Recently, a consistent theory to describe the current-driven motion of a single Néel wall was given,[12] where importance of the so-called quasi-zero-mode coordinate was stressed. In this paper, along with the same pathway as developed in Ref. 12, we consider a problem of current-driven sliding motion of the MKC in a chiral helimagnet coupled to the spin-polarized current. In Sec. II, we summarize physical properties of the MKC. In Sec. III, we derive coupled equations of motion (EOMs) for the collective coordinate of the center-of-mass motion and the localized quasi-zero-mode coordinate perpendicular to the helical plane. In Sec. IV, we give microscopic analysis of the conduction electrons under the electric field. In Sec. V, we derive the sliding conductivity of the MKC under an applied electric field. Then we demonstrate that the correlated dynamics is understood through a hierarchy of two relaxation times, i.e., Boltzmann relaxation time of conduction electrons, τ_{el}, and Gilbert damping time of the MKC, τ_{MKC}. We conclude our results in Sec. VI.

II. SLIDING MOTION OF THE MKC

In this section we summarize physical properties of the MKC.[21]

A. Formation of the MKC state

The MKC formation is described by the effective one-dimensional Hamiltonian (energy per unit area) in the continuum limit[21]

$$\mathcal{H}_{\mathrm{MKC}} = \frac{JS^2}{2a_0}\int_0^L dz[\partial_z \boldsymbol{n}(z)]^2 - \frac{S^2}{a_0^2}\int_0^L dz \boldsymbol{D}\cdot\boldsymbol{n}(z)\times\partial_z\boldsymbol{n}(z) - \frac{S}{a_0^3}\int_0^L dz\tilde{\boldsymbol{H}}\cdot\boldsymbol{n}(z). \tag{1}$$

By "effective one dimension," we mean that the magnetization exhibits no detectable variation in the xy plane over macroscopic scales. A local spin is described by a semiclassical vector $\boldsymbol{S}=S\boldsymbol{n}$ which is assumed to be slowly varying functions of one-dimensional coordinate z. a_0 is the cubic lattice constant of the constituent crystallographic lattice unit and L denotes the linear dimension of the system. The first term of Eq. (1) represents the ferromagnetic coupling with the strength $J>0$. The second term represents the DM interaction between the nearest neighbors,[25] characterized by the monoaxial vector $\boldsymbol{D}=D\hat{\boldsymbol{e}}_z$ along a certain crystallographic chiral axis (taken as the z axis) which coincides with the helical axis. Hamiltonian (1) is the same as the model treated by Liu[26] except that we ignore the single-ion anisotropy energy. Once we take into account the easy-axis type anisotropy term, $-K\Sigma_i(S_i^x)^2$, the mean-field ground-state configuration becomes either the chiral helimagnet for $K<D^2/J$ or the Ising ferromagnet for $K>D^2/J$. In this paper, we assume $K=0$ and left an effect of K for a future study. The third term is the Zeeman coupling with the magnetic field applied *perpendicular* to the chiral axis

$$\tilde{\boldsymbol{H}} = \tilde{H}\hat{\boldsymbol{e}}_x, \tag{2}$$

where $\tilde{H}=2\mu_B H$ (μ_B is the Bohr magneton and H is an applied field strength). In zero field, the long-period incommensurate helimagnetic structure with the modulation wave number

$$q_0 = a_0^{-1}\arctan\left(\frac{D}{J}\right) \simeq \frac{D}{a_0 J}, \tag{3}$$

where $(D \ll J)$ is stabilized with the definite chirality fixed by the direction of the monoaxial $\boldsymbol{D}$ vector.

Representing a unit-vector field as

$$\boldsymbol{n} = [\sin\theta(z)\cos\varphi(z), \sin\theta(z)\sin\varphi(z), \cos\theta(z)] \tag{4}$$

by the polar coordinates $\theta(z)$ and $\varphi(z)$ [Fig. 1(b)], Hamiltonian (1) becomes the generalized sine-Gordon Hamiltonian

$$\mathcal{H}_{\mathrm{MKC}} = \frac{JS^2}{a_0}\int_0^L dz \times\left[\frac{1}{2}\theta_z^2 + \frac{1}{2}\sin^2\theta\varphi_z^2 - q_0\sin^2\theta\varphi_z - m^2\sin\theta\cos\varphi\right], \tag{5}$$

where the first breather mass m with a physical dimension of inverse length, $[L^{-1}]$, is given by

$$m^2 = \frac{\tilde{H}}{JSa_0^2}. \tag{6}$$

As a stationary configuration which minimizes $\mathcal{H}_{\mathrm{MKC}}$, we obtain the MKC state described by

$$\boldsymbol{n}_0(z) = [\cos\varphi_0(z), \sin\varphi_0(z), 0], \tag{7}$$

where

$$\cos\left(\frac{\varphi_0(z)}{2}\right) = \mathrm{sn}\left(\frac{m}{\kappa}z\right) \tag{8}$$

with "sn" being the Jacobi-sn function. The length

$$L_{\text{kink}} = \frac{2\kappa K(\kappa)}{m} \tag{9}$$

represents the spatial period of the MKC. Hereinafter, $K(\kappa)$ and $E(\kappa)$ denote the elliptic integrals of the first and second kinds, respectively, with the elliptic modulus κ $(0 \le \kappa \le 1)$. The modulus κ is determined by minimizing $\mathcal{H}_{\text{MKC}}$ with respect to κ to give

$$\frac{m}{\kappa} = \frac{\pi q_0}{4E(\kappa)}. \tag{10}$$

Equations (6) and (10) give the critical field strength $\tilde{H}_c = JS(\pi q_0 a_0/4)^2$, which amounts to 1 kOe for chiral helimagnet $Cr_{1/3}NbS_2$.[27,28] The incommensurate MKC state is stabilized for $\tilde{H} < \tilde{H}_c$. Upon increasing $\tilde{H}$ from zero, the IC-to-C phase transition from the MKC state to the forced ferromagnetic state occurs at $\tilde{H} = \tilde{H}_c$ (corresponding to $\kappa = 1$) at which L_{kink} diverges. In the zero-field limit when $\kappa = 0$, $K(0) = E(0) = \pi/2$ retrieves $L_{\text{kink}} = 2\pi/q_0$.

B. Elementary excitations, zero mode, and quasizero mode

To consider the sliding motion of the MKC, we should keep in mind that there is no physical field which has a direct coupling with the MKC. So, the motion of the MKC requires internal deformation, i.e., we need information on the elementary excitations. To see this, we introduce the $\delta\theta(z,t)$ (out-of-plane) and $\delta\varphi(z,t)$ (in-plane) fluctuations of the local spins around the stationary MKC configuration $\boldsymbol{n}_0(z)$, i.e., $\varphi(z,t) = \varphi_0(z) + \delta\varphi(z,t)$ and $\theta(z,t) = \pi/2 + \delta\theta(z,t)$. The terms "out-of-plane" and "in-plane" are used with respect to the helical (xy) plane [see Fig. 1(b)]. By expanding $\mathcal{H}_{\text{MKC}}$ up to the second order with respect to the $\delta\theta$ and $\delta\varphi$, $\mathcal{H}_{\text{MKC}}[\theta,\varphi] = \mathcal{H}_{\text{MKC}}[\theta_0,\varphi_0] + \delta\mathcal{H}_{\text{MKC}}$, we have

$$\delta\mathcal{H}_{\text{MKC}} = \int dz (\delta\theta \hat{\Lambda}_\theta \delta\theta + \delta\varphi \hat{\Lambda}_\varphi \delta\varphi). \tag{11}$$

Here the linear differential operators are given by

$$\hat{\Lambda}_\theta = -\frac{JS^2}{2a_0}\partial_z^2 + \frac{\tilde{H}S}{2a_0^3}\cos\varphi_0 - \frac{JS^2}{2a_0}(\partial_z\varphi_0)^2 + \frac{JS^2}{a_0}q_0(\partial_z\varphi_0), \tag{12a}$$

$$\hat{\Lambda}_\varphi = -\frac{JS^2}{2a_0}\partial_z^2 + \frac{\tilde{H}S}{2a_0^3}\cos\varphi_0. \tag{12b}$$

The eigenvalue problem for these operators corresponds to the Jacobi form of the Lamé equation. The fluctuations are spanned by the orthogonal eigenfunctions $v_q(z)$ and $u_q(z)$,

$$\varphi(z,t) = \varphi_0(z) + \sum_q \eta_q(t) v_q(z), \tag{13}$$

$$\theta(z,t) = \pi/2 + \sum_q \xi_q(t) u_q(z), \tag{14}$$

where $\int_0^L |v_q(z)|^2 dz = \int_0^L |u_q(z)|^2 dz = 1$. The time-dependent eigenmode coordinates $\eta_q(t)$ and $\xi_q(t)$ play role of dynamical variables. The physical dimension of v_q and u_q is $[L^{-1/2}]$ and that of η_q and ξ_q is $[L^{1/2}]$. These functions are all labeled by the quasimomentum q (Floquet index). Explicit forms of v_q and u_q are given in Ref. 21.

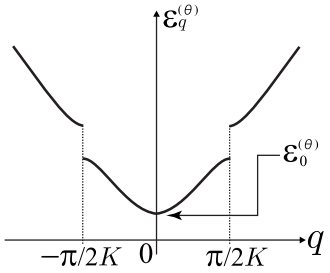

FIG. 2. The energy dispersion of the eigenmodes for the out-of-plane θ-fluctuations $(\varepsilon_q^{(\theta)})$.

Then, the fluctuation part $\delta\mathcal{H}_{\text{MKC}}$ is diagonalized to give

$$\delta\mathcal{H}_{\text{MKC}} = a_0^{-3}\sum_q [\varepsilon_q^{(\varphi)}\eta_q^2(t) + \varepsilon_q^{(\theta)}\xi_q^2(t)], \tag{15}$$

which describes the MKC phonon modes.[23] Both $\varepsilon_q^{(\varphi)}$ and $\varepsilon_q^{(\theta)}$ comprise the "acoustic" and "optical" bands.[29] The acoustic band is formed out of correlated translations of the individual kinks while the optical band corresponds to renormalized Klein-Gordon bosons. In Fig. 2, the dispersion relation of $\varepsilon_q^{(\theta)}$ is shown.

An essential feature is that the φ mode is gapless $(\varepsilon_0^{(\varphi)} = 0)$ but the θ mode acquires an energy gap given by

$$\varepsilon_0^{(\theta)} = JS^2 a_0^2 \frac{m^2}{\kappa^2}\bar{\Delta} \simeq \frac{D^2S^2}{2J}, \tag{16}$$

where

$$\bar{\Delta} = \int_0^L dz \Delta(z) u_0^2(z) \tag{17}$$

with

$$\Delta(z) = (8/\pi)E(\kappa)\mathrm{dn}\left(\frac{m}{\kappa}z\right) - 2\mathrm{dn}^2\left(\frac{m}{\kappa}z\right). \tag{18}$$

The presence of this energy gap is essential to produce the inertial mass of the MKC.[21] The normalized wave function at the bottom of the acoustic band $(q = 0)$ is

$$v_0(z) = u_0(z) = L^{-1/2}\sqrt{\frac{K(\kappa)}{E(\kappa)}}\mathrm{dn}\left(\frac{2K(\kappa)}{L_{\text{kink}}}z\right)$$

$$= L^{-1/2}\frac{2}{\pi q_0}\sqrt{K(\kappa)E(\kappa)}\partial_z\varphi_0(z) \tag{19}$$

with "dn" being the Jacobi-dn function. $v_0(z)$ and $u_0(z)$, respectively, corresponds to the zero mode and quasizero mode which are localized around each kink.[21] In conventional terminology, the zero mode means a mode excited with no excess energy. In the present case, the in-plane $v_0(z)$ mode exactly corresponds to this case, but the out-of-plane $u_0(z)$ zero mode acquires the gap given by Eq. (16). By this reason, we call $u_0(z)$-mode "quasizero mode."[12]

C. Collective coordinates: Quasi-zero-mode and out-of-plane zero-mode coordinates

In the continuum limit, the MKC configuration has continuous degeneracy related with a choice of the center-of-mass position, Z, of the MKC.[30] This degeneracy apparently leads to *rigid* translation of the MKC, i.e.,

$$\boldsymbol{n}_0(z) \to \boldsymbol{n}_0(z-Z). \tag{20}$$

As shown in Ref. 21, the translation in off-equilibrium accompanies *internal deformation* of the MKC which is analogous to the Döring's mechanism of the DW motion.[13] In order to describe correct local spin dynamics, one has to regard the parameter Z as a dynamical variable $Z(t)$ and replace the zero mode (Nambu-Goldstone) coordinate η_0 with $Z(t)$.[31] Following this procedure, the mode expansions in Eqs. (13) and (14) are promoted to

$$\varphi(z,t) = \varphi_0[z-Z(t)] + \sum_{q\neq 0} \eta_q(t) v_q[z-Z(t)], \tag{21a}$$

$$\theta(z,t) = \pi/2 + \xi_0(t) u_0[z-Z(t)] + \sum_{q\neq 0} \xi_q(t) u_q[z-Z(t)]. \tag{21b}$$

In these expansions, only the quasizero mode u_0 contributes to the inertial mass of the MKC.[21] That is to say, to describe sliding motion of the MKC, it is enough to include only $Z(t)$ and $\xi_0(t)$ as dynamical variables (canonical coordinates). This treatment is analogous to ignoring the spin-wave contribution in the DW dynamics.[12] Based on this fact, we ignore all the terms with finite q in Eqs. (21a) and (21b) and simply write

$$\varphi(z,t) = \varphi_0[z-Z(t)], \tag{22a}$$

$$\theta(z,t) = \pi/2 + \xi_0(t) u_0[z-Z(t)]. \tag{22b}$$

Then, Eq. (15) is simplified to give

$$\delta\mathcal{H}_{\mathrm{MKC}} = a_0^{-3}\varepsilon_0^{(\theta)}\xi_0^2(t), \tag{23}$$

These equations are essentially the same as Eqs. (9) and (10) of Ref. 12. As in the case of DW motion, we naturally include the out-of-plane quasizero (OPQZ) mode, in addition to the in-plane (φ) zero mode replaced by $Z(t)$. The zero-mode wave function $u_0[z-Z(t)]$ serves as the basis function of the θ fluctuations localized around each kink and $\xi_0(t)$ is the OPQZ *coordinate*. Then, our effective theory is fully described by two dynamical variables $Z(t)$ and $\xi_0(t)$ which play a role of physical coordinates along the Hilbert space of the orthogonal θ and φ fluctuations. As shown in Ref. 21, we have $\xi_0(t)\neq 0$ only for nonequilbrium state where the MKC exhibits sliding motion. An emergence of such coherent collective transport in nonequilibrium state is a manifestation of the dynamical off-diagonal long-range order.

III. EQUATIONS OF MOTION OF THE MKC

A. sd interaction

Next, we consider the coupling of the MKC with the itinerant quantum spins via the sd coupling described by the Hamiltonian

$$\mathcal{H}_{\mathrm{sd}} = -\frac{SJ_{\mathrm{sd}}}{a_0^3}\int_0^L dz\hat{\boldsymbol{s}}(z)\cdot\boldsymbol{n}[\theta,\varphi], \tag{24}$$

where J_{sd} represents the sd coupling strength. The electron spin

$$\hat{\boldsymbol{s}}(z) = \frac{1}{2}c_\sigma^\dagger(z)\boldsymbol{\sigma}_{\sigma\sigma'}c_{\sigma'}(z) \tag{25}$$

is fully quantum-mechanical operator with $c_\sigma^\dagger$ (c_σ) being the electron creation (annihilation) operator and $\boldsymbol{\sigma}$ being the vector Pauli matrices. Since it is difficult to make quantitative estimation of J_{sd} in real materials, we should regard Hamiltonian (24) as a working assumption to simulate the interaction between the local spins and itinerant spins.

To understand the effect of the sd coupling, it is useful to note

$$\boldsymbol{n}[\theta,\varphi] \simeq \left(1-\frac{1}{2}\delta\theta^2\right)\boldsymbol{n}_0 - \hat{\boldsymbol{e}}_z\delta\theta, \tag{26}$$

where we retain terms appearing in Eqs. (22a) and (22b). Plugging this into Eq. (24) and using Eqs. (22a) and (22b), we immediately have

$$\mathcal{H}_{\mathrm{sd}} = -\frac{J_{\mathrm{sd}}S}{a_0^3}\left(\mathcal{F}_0[Z(t)] - \frac{1}{2}\mathcal{F}_2[Z(t)]\xi_0^2(t)\right) + \frac{J_{\mathrm{sd}}S}{a_0^3}\mathcal{F}_1[Z(t)]\xi_0(t), \tag{27}$$

where

$$\mathcal{F}_0[Z(t)] = \int_0^L dz\{\hat{\boldsymbol{s}}(z)\cdot\boldsymbol{n}_0[z-Z(t)]\}, \tag{28a}$$

$$\mathcal{F}_1[Z(t)] = \int_0^L dz\hat{s}^z(z)u_0[z-Z(t)], \tag{28b}$$

$$\mathcal{F}_2[Z(t)] = \int_0^L dz\{\hat{\boldsymbol{s}}(z)\cdot\boldsymbol{n}_0[z-Z(t)]\}\times\{u_0[z-Z(t)]\}^2, \tag{28c}$$

which are functions of $Z(t)$.

We note that at this stage, $\hat{\boldsymbol{s}}(z)$ is still a quantum-mechanical operator. When we consider the effective Lagrangian, we need to integrate out electron degrees of freedom under an applied electric field. This procedure is incorporated by replacing $\mathbf{s}(z)$ with its statistical average $\langle\mathbf{s}(z)\rangle$. As we show below, we eventually have $\langle\hat{s}^z(z)\rangle=0$, i.e.,

$$\langle\mathcal{F}_1[Z(t)]\rangle = 0. \tag{29}$$

Therefore, we have

$$\mathcal{H}_{\rm sd} = -\frac{J_{\rm sd}S}{a_0^3}\left(\langle \mathcal{F}_0[Z(t)]\rangle - \frac{1}{2}\langle \mathcal{F}_2[Z(t)]\rangle \xi_0^2\right), \tag{30}$$

where the statistical average over the electron degrees of freedom is denoted by $\langle\cdots\rangle$. To compute this average, we need a nonequilibrium (Keldysh) Green's function technique (see Sec. IV).

B. Lagrangian

To set up EOM, we need a Lagrangian,

$$\mathcal{L} = \mathcal{L}_{\rm B} - \delta\mathcal{H}_{\rm MKC} - \mathcal{H}_{\rm sd}, \tag{31}$$

including kinetic Berry phase term

$$\mathcal{L}_{\rm B} = \frac{\hbar S}{a_0^3}\int_0^L dz(\cos\,\theta - 1)\varphi_t = \frac{\hbar S}{a_0^3}\mathcal{K}\xi_0(t)\dot{Z}(t), \tag{32}$$

where we used Eqs. (21a) and (21b) and introduced

$$\mathcal{K} = \int_0^L dz u_0(z)\partial_z\varphi_0 \simeq q_0\sqrt{L}, \tag{33}$$

under the condition of weak-field limit, $\kappa \ll 1$. Putting together Eqs. (23), (30), and (32), we have

$$S^{-1}a_0^3\mathcal{L} = \hbar\mathcal{K}\xi_0(t)\dot{Z}(t) - \varepsilon_0^{(\theta)}S^{-1}\xi_0^2(t) + J_{\rm sd}\left(\langle \mathcal{F}_0[Z(t)]\rangle - \frac{1}{2}\langle \mathcal{F}_2[Z(t)]\rangle\xi_0^2(t)\right). \tag{34}$$

This Lagrangian has simple physical meaning. The first term represents the kinetic energy carried by the MKC. The second term represents the restoring force by the DM interaction which acts like an effective easy-plane anisotropy energy. The third term represents the spin torque transferred from the itinerant spins to the local moments.

C. Euler-Lagrange-Rayleigh equations of motion

To incorporate the damping effect in the Lagrangian formalism, we utilize the Rayleigh dissipation function $\mathcal{W}=[\hbar\alpha S^2/(2Sa_0^3)]\int_0^L dz[d\boldsymbol{n}(z)/dt]^2$ written as

$$S^{-1}a_0^3\mathcal{W} = \frac{\alpha\hbar}{2}[\mathcal{M}\dot{Z}^2(t) + \dot{\xi}_0^2(t)], \tag{35}$$

where

$$\mathcal{M} = \int_0^L dz[\partial_z\varphi_0(z)]^2 \simeq q_0^2 L. \tag{36}$$

Using Eqs. (34) and (35), we write down the Euler-Lagrange-Rayleigh equations of motion for the variables Z and ξ_0. We obtain

$$\hbar\mathcal{K}\dot{\xi}_0(t) - J_{\rm sd}(\partial_Z\langle \mathcal{F}_0[Z(t)]\rangle) = -\alpha\hbar\mathcal{M}\dot{Z}(t), \tag{37a}$$

$$-\hbar\mathcal{K}\dot{Z}(t) + 2S^{-1}\varepsilon_0^{(\theta)}\xi_0(t) + J_{\rm sd}\langle \mathcal{F}_2[Z(t)]\rangle\xi_0(t) = -\alpha\hbar\dot{\xi}_0(t). \tag{37b}$$

These EOMs contain only terms linear in the dynamical variables Z and ξ_0 and are precisely the same as those proposed in Ref. 21 with modifications by the presence of the sd interaction and the dissipation term.

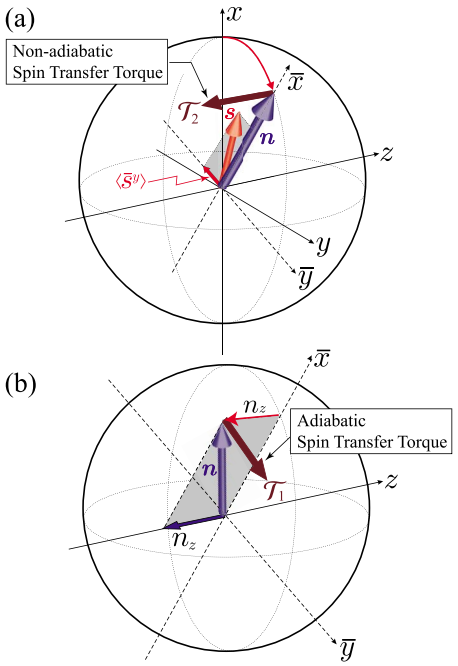

FIG. 3. (Color online) (a) The nonadiabatic STT, $\mathcal{T}_2$, owing to the TSA $\langle\bar{s}^y\rangle$ along the local $\bar{y}$ axis, and (b) the adiabatic STT $\mathcal{T}_1$ owing to the OPQZA (n_z).

D. Transversal spin accumulation and nonadiabatic spin-transfer torque

In Eq. (37a), there appear the coefficient

$$\partial_Z\langle \mathcal{F}_0[Z(t)]\rangle = -\int_0^L dz\left(\hat{\boldsymbol{s}}(z)\cdot\frac{\partial}{\partial z}\boldsymbol{n}_0[z - Z(t)]\right) \simeq -q_0\mathcal{T}_2, \tag{38}$$

where we used the relation $\partial_z\varphi_0 \simeq q_0$ and introduced the nonadiabatic STT on the local moments

$$\mathcal{T}_2 = \int_0^L dz\hat{\mathbf{e}}_z\cdot[\boldsymbol{n}_0(z)\times\langle\mathbf{s}(z)\rangle]. \tag{39}$$

The physical dimension of $\mathcal{T}_2$ is $[L]$. It is useful to note that $\mathcal{T}_2=0$ if $\boldsymbol{n}_0(z)$ and $\langle\mathbf{s}(z)\rangle$ are parallel to each other. To see physical meaning of $\mathcal{T}_2$, we perform the local gauge transformation for the conduction-electron creation operator in a spinor form, $c^\dagger=(c_\downarrow^\dagger, c_\uparrow^\dagger)$,

$$c(z) \to a(z) = \hat{U}(z)c(z) \tag{40}$$

with the unitary operator

$$\hat{U}(z) = \exp[i\sigma_z\varphi_0(z)]. \tag{41}$$

By this transformation, the laboratory frame xyz is transformed to local frame $\bar{x}\bar{y}\bar{z}$, where the equilibrium local moment $\boldsymbol{n}_0(z)$ points in the direction of $\bar{x}$ axis [see Fig. 3]. Consequently, the STT is written as

$$\mathcal{T}_2 = \frac{1}{2}\int_0^L dz\langle a^\dagger(z)\sigma^y a(z)\rangle = \frac{1}{2}\sum_k \langle a_k^\dagger \sigma^y a_k\rangle \equiv L\langle \bar{s}^y\rangle, \tag{42}$$

where $a^\dagger=(a_\uparrow^\dagger, a_\downarrow^\dagger)$ is the spinor of electron creation operators and the Fourier transform $a(z)=1/\sqrt{L}\Sigma_k e^{ikz}a_k$ was introduced. The operator $a(z)$ is dimensionless while a_k has a dimension of $[L^{1/2}]$.

As indicated in Fig. 3(a), this means that $\mathcal{T}_2$ originates from the mistracking between the conduction-electron spin and the spatially varying local moments.[10] When the electrons travel along the chiral axis, they see the local moments continuously rotating over length scales much longer than the atomic scale. In this process, the electrons cannot instantly follow the background local moments and there arises accumulation of the component of the electron spin which is perpendicular to the local moment, i.e., TSA occurs.[10] As a consequence of this process, the local moments feels the torque $\mathcal{T}_2$ and rotate to give the out-of-plane canting (finite $\delta\theta$).

E. Longitudinal spin depletion

Next, in Eq. (37b), there appears the coefficient

$$\langle \mathcal{F}_2[Z(t)]\rangle \simeq L^{-1}\mathcal{S}_\parallel, \tag{43}$$

where we introduced the *longitudinal spin depletion* (LSD)

$$\mathcal{S}_\parallel = \int_0^L dz \boldsymbol{n}_0(z)\cdot\langle \mathbf{s}(z)\rangle. \tag{44}$$

The physical dimension of $\mathcal{S}_\parallel$ is $[L]$. Similarly, performing the gauge transformation Eq. (41), the LSD is written as

$$\mathcal{S}_\parallel = \frac{1}{2}\int_0^L dz\langle a^\dagger(z)\sigma^x a(z)\rangle = \frac{1}{2}\sum_k \langle a_k^\dagger \sigma^x a_k\rangle \equiv L\langle \bar{s}^x\rangle. \tag{45}$$

Below, we quantitatively estimate $\mathcal{T}_2$ and $\mathcal{S}_\parallel$ (see Sec. IV C).

Now, the physical meaning of Eqs. (37a) and (37b) is clear. In the left-hand side of Eq. (37a) the first term represents the inertial motion of the MKC. The second term represents the constant driving force (STT) acting on the MKC. The right-hand side represents the linear drag effect, which eventually balance with the driving force given by the STT. In the left-hand side of Eq. (37b) the first term represents the linear translation of the MKC as a whole. The second term represents the restoring force given by the DM interaction. The third term represents the constant STT.

F. Relaxational dynamics of the MKC

Using Eqs. (33), (36), (38), and (43) the coupled EOMs [Eqs. (37a) and (37b)] become

$$\dot{\xi}_0(t) = -\frac{1}{\hbar(1+\alpha^2)}\left\{\alpha(2S^{-1}\varepsilon_0^{(\theta)} + J_{\rm sd}L^{-1}\mathcal{S}_\parallel)\xi_0(t) + \frac{J_{\rm sd}}{\sqrt{L}}\mathcal{T}_2\right\}, \tag{46}$$

$$\dot{Z}(t) = \frac{1}{\hbar q_0\sqrt{L}(1+\alpha^2)}\left\{(2S^{-1}\varepsilon_0^{(\theta)} + J_{\rm sd}L^{-1}\mathcal{S}_\parallel)\xi_0(t) - \frac{J_{\rm sd}}{\sqrt{L}}\alpha\mathcal{T}_2\right\}. \tag{47}$$

In what follows we neglect the $\mathcal{S}_\parallel$ contribution, which is multiplied by the factor $1/L$ whereas $\mathcal{T}_2$ enters with $1/\sqrt{L}$ [see also discussion given in Sec. IV C and Fig. 6(c)]. Let us switch on the electric field E at $t=0$ and take the initial condition $\xi_0(0)=0$, i.e., the whole MKC is assume to be static at $t=0$. Then, Eqs. (46) and (47) are easily solved to give the relaxation solution

$$\xi_0(t) = \xi_0^*(1-e^{-t/\tau_{\rm MKC}}), \tag{48}$$

$$\dot{Z}(t) = V^*(1-e^{-t/\tau_{\rm MKC}}), \tag{49}$$

where the terminal value of the quasi-zero-mode coordinate is

$$\xi_0^* = -\frac{J_{\rm sd}\mathcal{T}_2}{\alpha\sqrt{L}(2S^{-1}\varepsilon_0^{(\theta)} + J_{\rm sd}L^{-1}\mathcal{S}_\parallel)} \tag{50}$$

and the terminal velocity of the MKC is

$$V^* = -\frac{\alpha^{-1}J_{\rm sd}}{\hbar q_0 L}\mathcal{T}_2. \tag{51}$$

The relaxation time is given by

$$\tau_{\rm MKC} = \frac{\hbar(\alpha^{-1}+\alpha)}{2S^{-1}\varepsilon_0^{(\theta)} + L^{-1}J_{\rm sd}\mathcal{S}_\parallel} \simeq \frac{\hbar(\alpha^{-1}+\alpha)}{SJ}\left(\frac{J}{D}\right)^2, \tag{52}$$

where $L^{-1}J_{\rm sd}\mathcal{S}_\parallel$ is negligibly smaller than the energy scale of $\varepsilon_0^{(\theta)}$. Taking $J=10$ K$\simeq 10^{-22}$ J, $D/J=10^{-1}$, $\alpha\simeq 10^{-2}$, and $S=1$, we obtain $\tau_{\rm MKC}\simeq 10^{-9}$ s.

The result in Eq. (50) implies that upon a switching of an external electric field the TSA, $\langle \bar{s}_y\rangle$, along the local $\bar{y}$ axis appears and creates a spin torque, which causes a precession of the local magnetic moment around the $\bar{y}$ axis and consequently produces a finite deviation of the polar angle $\delta\theta=\theta-\theta_0$. We call this process OPQZ *accumulation* (OPQZA) schematically depicted in Fig. 3(b). The important consequence of the OPQZA is an emergence of the finite out-of-plane (z) component of the local spin

$$n_z(z,t) = \cos\,\theta(z,t) \simeq -\xi_0^* u_0[z-Z(t)]. \tag{53}$$

This effect is physically similar to an emergence of a demagnetization field phenomenologically introduced by Döring,[13] and Slonczewski.[1]

The adiabatic spin-transfer torque related with the OPZA [see Fig. 3(b)] is given by

$$\mathcal{T}_1 = \int_0^L dz\hat{\mathbf{e}}_y\cdot[\boldsymbol{n}(z)\times\boldsymbol{n}_z(z)] \tag{54}$$

and amounts to $\mathcal{T}_1\approx\xi_0^*\sqrt{L}$ in the small-field limit.

By using Eqs. (16) and (50) we obtain the important ratio

$$\left|\frac{\mathcal{T}_1}{\mathcal{T}_2}\right| \approx \frac{JJ_{\rm sd}}{\alpha D^2 S}. \tag{55}$$

Given the above estimations the quantity turns out to be of order 10^5. One sees that the nonadiabatic spin-transfer torque is converted into the amplified adiabatic STT. The later enables to push such a heavy macroscopic object as the soliton lattice is.

It is essential that the Gilbert damping coefficient, α, enters Eq. (52). The relaxation process of the MKC dynamics is governed by the Boltzmann relaxation followed by the Gilbert damping in hierarchical manner. It is crucial to recognize that the quasi-zero-mode coordinate ξ_0 acquires finite value (i.e., OPQZA) only for the current flowing state which is nonequilibrium but stationary. *This is the case where dynamical relaxation leads to finite accumulation of physical quantities which are zero in equilibrium.* This situation is totally analogous to the case of a single DW.[32]

IV. CONDUCTION ELECTRONS

In the previous section, the relaxational solutions are expressed in terms of $\mathcal{T}_2$ and $\mathcal{S}_\parallel$ given by Eqs. (42) and (45), respectively. To compute these quantities, we need to consider the electron degrees of freedom.

A. Magnetic field conditions

We consider relaxational dynamics of conduction electrons under the electric field $\mathbf{E}=E\hat{\mathbf{e}}_z$ and magnetic field $\tilde{\boldsymbol{H}}=\tilde{H}\hat{\mathbf{e}}_x$. Here we try to fix the weak magnetic field condition, i.e., mutual relation among E, $\tilde{H}$, and the Boltzmann relaxation time $\tau_{\rm el}$. In the following arguments, we consider the case where electrons move almost parallel to $\mathbf{E}$ and assume that deviation of the orbital motion away from the direction of $\mathbf{E}$ can be neglected. This condition is fulfilled by

$$\omega_c \tau_{\rm el} \ll 1, \tag{56}$$

where $\omega_c=eB/m$ (B is the magnetic flux density in SI unit) denotes the electron cyclotron resonance frequency. In the opposite limit, $\omega_c\tau_{\rm el}\gtrsim 1$, cyclotron resonance occurs, which must be avoided here. In our case, it is appropriate for a clean metal to assume $\tau_{\rm el}\sim 10^{-11}$ s at very low temperature and $\tau_{\rm el}\sim 10^{-14}$ s at room temperatures. Then, the condition in Eq. (56) is satisfied by

$$H \ll 10^4 - 10^7 \ \text{Oe}. \tag{57}$$

Fortunately, this weak field condition is well satisfied because the critical-field strength H_c usually amounts to atmost 1 kOe. More strictly speaking, we should limit our argument to the case of $H \ll H_c$. Throughout this paper, we use this criteria as the weak-field condition.

Here we comment on the physical meaning of the weak-field limit. It is to be stressed that the limit $H\to 0$ is never smoothly connected to the case of $H=0$. In the case of $H=0$ where the background system becomes a simple spiral state, translational motion of the background does not make any sense, because apparent translation is nothing more than global rotation of the whole spiral structure associated with gauge freedom (or masless Goldstone mode). So, there is no analog of our quasizero-mode associated with θ fluctuations. In another word, translation and rotation cannot be decoupled in a simple spiral state. In the discussion below, we take $H\to 0$ limit to consider conduction electrons. This treatment may cause unnecessary annoyance that our treatment is not self-consistent. But, it is important to bear in mind that taking $H\to 0$ limit for conduction electron is totally different from putting $H=0$ for the ground state of the background structure. As shown below, conduction electron produces torque and the background responds to this with finite intertia. In the case of simple spiral, there is no inertia and the background responds in singular manner. Only extrinsic pinning (which gives rise to artificial field to fix the gauge) can rescue this catastrophe.

B. Background MKC, gauge field, and phase shift

For simplicity, we use the one-dimensional (1D) tight-binding model described by the kinetic term

$$\mathcal{H}_{\rm kin} = a_0^{-3}\sum_\delta t_\delta \int_0^L dz c^\dagger(z) c(z+\delta) + \text{H.c.}, \tag{58}$$

where $c_\sigma^\dagger(c_\sigma)$ are the electron creation (annihilation) operators with spin $\sigma=\uparrow,\downarrow$. The hopping integral between adjacent sites separated by δ is denoted by t_δ. Since the period of the MKC ($q_0^{-1}\simeq 100$ nm) is much larger than an electron wavelength ($\sim$0.5 nm), the MKC is regarded as a very smooth background for the electrons. Consequently, it is legitimate to ignore reflection of the electrons by the MKC.[33] For a description of electron transport in such a slowly varying magnetization field, it is suitable to represent the electron degrees of freedom in the rotated local frame $\overline{xyz}$ reached from the crystal frame xyz by the gauge transformation Eq. (41).[34,35] In the rotated frame, the kinetic energy term in Eq. (58) acquires the Peierls phase written as

$$\mathcal{H}_{\rm kin} = a_0^{-3}\sum_\delta t_\delta \int_0^L dz a^\dagger(z) e^{i/2\sigma^z[\varphi_0(z)-\varphi_0(z+\delta)]} a(z+\delta) + \text{H.c.} \tag{59}$$

Another aspect on t_δ comes from the condition that the relevant time scales of the electron hopping $\hbar/t_\delta$ should be much less than that of the slowly varying local moments $\hbar/J$. This condition of adiabaticity leads to the necessary requirement $D<J_{\rm sd}<J\ll t_\delta$.

Under the condition in Eq. (56), the wave number k along z axis is regarded as a good quantum number. Performing the Fourier transform $a(z)=L^{-1/2}\Sigma_k e^{ikz}a_{k\sigma}$ and noting

$$\varphi_0(z) - \varphi_0(z+\delta) \simeq -q_0\delta, \tag{60}$$

for small $\tilde{H}_y$. Then, Hamiltonian (59) indicates that the traveling electrons see the SU(2) gauge field $\hat{\mathcal{A}}_z=-q_0\delta\sigma^z/2$ along the helical axis. Meaning of this gauge field is easily understood as follows. Let us assume the adiabatic limit where the itinerant spins perfectly follow the background local spins. Then, the itinerant spins rotate clockwise or an-

ticlockwise depending on the chirality of the helical magnetic order. This rotation is interpreted to be caused by the fictitious magnetic field along the helical axis. This fictitious field give the gauge field $\hat{\mathcal{A}}_z$.

Now, we easily diagonalize $\mathcal{H}_{\rm kin}$ to give

$$\mathcal{H}_{\rm kin} = a_0^{-3}\sum_{k,\sigma} \varepsilon_{k\sigma} a_{k\sigma}^{\dagger} a_{k\sigma}, \tag{61}$$

where

$$\varepsilon_{k\sigma} = 2\sum_{\delta} t_{\delta} \cos\left[\left(k - \frac{\sigma}{2}q_0\right)\delta\right] \tag{62}$$

with $\sigma=+$ (for $\uparrow$) and $-$ (for $\downarrow$). It is important to stress that the MKC is a *periodic* background for the itinerant spins while the DW is a localized one.[12] So, the coupling of the conduction electrons with the MKC simply gives rise to a *phase shift* $k \to k \pm q_0/2$.

C. Microscopic computation of $\mathcal{T}_2$ and $\mathcal{S}_{\parallel}$

The gauge transformation Eq. (41) transforms the sd Hamiltonian (24) to the form given by

$$\mathcal{H}_{\rm sd} = -\frac{SJ_{\rm sd}}{a_0^3}\int_0^L dz \bar{s}^x(z), \tag{63}$$

where $\bar{s}^x(z)=\frac{1}{2}a^{\dagger}(z)\sigma^x a(z)$. The local moment $\boldsymbol{n}_0$ is directed along the local $\bar{x}$ axis in the rotating frame.

Here we note that by means of exact diagonalization of the electron Hamiltonian $\mathcal{H}_{\rm el}=\mathcal{H}_{\rm kin}+\mathcal{H}_{\rm sd}$ one can easily verify that no transversal s^y component emerges, i.e., no nonadiabatic STT arises in an isolated system. To organize a nonzero spin accumulation an external electric field should be applied that produces an electric current through the helimagnet and creates a nonequilibrium state in the electron subsystem.

To compute $\mathcal{T}_2$ and $\mathcal{S}_{\parallel}$, we exploit the technique of nonequilbrium Green's functions.[36] A variant of the method based on equations of motion (EOMs) for Keldysh's functions developed in Ref. 37 is adequate here. Now, $\mathcal{T}_2$ and $\mathcal{S}_{\parallel}$ are, respectively, written as

$$\mathcal{T}_2 = L\sum_k \mathrm{Re}\, G^{<}_{k\uparrow,k\downarrow}(t,t), \tag{64a}$$

$$\mathcal{S}_{\parallel} = L\sum_k \mathrm{Im}\, G^{<}_{k\uparrow,k\downarrow}(t,t), \tag{64b}$$

where the lesser component of the path-oriented Green's function is defined by

$$G^{<}_{k\sigma,k'\sigma'}(t,t') = i\langle a^{\dagger}_{k'\sigma'}(t')a_{k\sigma}(t)\rangle, \tag{65}$$

where t (t') is defined on the upper (lower) branch of the Keldysh contour.[36]

What we need here is the lesser component of the contour-ordered Green's function $G^{<}_{k\sigma;k'\sigma'}(t,t')$. By treating the sd-interaction Eq. (63) as a perturbation, the Green's function is estimated in the lowest order Born approximation, we obtain

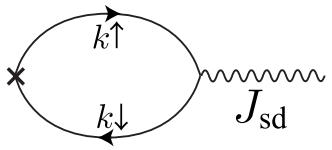

FIG. 4. Feynmann diagram representing the particle-hole polarization accompanying the spin flip caused by the s-d interaction (represented by wavy line) which leads to the nonadiabatic STT, $\mathcal{T}_2$. The solid line represents the electron/hole one-particle propagation, wavy line represents the gauge field caused by the background helical texture, and the cross represents the local spin.

$$G^{<}_{k\sigma;k'\sigma'}(t,t') \simeq i f_{k\sigma} e^{-i\varepsilon_{k\sigma}(t-t')}\delta_{kk'}\delta_{\sigma\sigma'} - i\frac{J_{\rm sd}S}{2}\left(\frac{f_{k\sigma}e^{-i\varepsilon_{k\sigma}(t-t')} - f_{k\sigma'}e^{-i\varepsilon_{k\sigma'}(t-t')}}{\varepsilon_{k\sigma-}\varepsilon_{k\sigma'} - i\delta}\right) \times \delta_{kk'}\sigma^x_{\sigma\sigma'}, \tag{66}$$

where $f_{k\sigma}$ is the distribution function ($\beta=1/T$) for the state labeled by the wave number k and spin σ. It is noted that the sd interaction gives rise to one-electron spin-flip process to give off-diagonal matrix elements $\langle a_k^{\dagger}\sigma^x a_k\rangle$ and $\langle a_k^{\dagger}\sigma^y a_k\rangle$. Then, we have $\langle a_k^{\dagger}\sigma^z a_k\rangle=0$ and

$$\mathcal{T}_2 = \frac{\pi J_{\rm sd}S}{2}L\sum_k (f_{k\uparrow} - f_{k\downarrow})\delta(\varepsilon_{k\uparrow} - \varepsilon_{k\downarrow}), \tag{67}$$

$$\mathcal{S}_{\parallel} = -\frac{J_{\rm sd}S}{2}L\sum_k \mathcal{P}\frac{f_{k\uparrow} - f_{k\downarrow}}{\varepsilon_{k\uparrow} - \varepsilon_{k\downarrow}}. \tag{68}$$

In Fig. 4, we depict particle-hole process contributing to the $\mathcal{T}_2$.

Here we comment on the condition under which the Born approximation is valid. As will be discussed in Sec. V B, the splitting of the conduction bands due to the gauge field should exceeds the magnitude of $J_{\rm sd}$ to justify perturbative treatment of $J_{\rm sd}$.

D. Boltzmann approximation

At the final step, we need to obtain an explicit form of the distribution function $f_{k\sigma}$ in the stationary current-flowing state. Let switch on the electric field $\mathbf{E}$ at $t=0$. We introduce the Boltzmann relaxation time $\tau_{\rm el}$. We assume that the deviation from equilibrium Fermi-Dirac distribution $f_0(\varepsilon_{k\sigma})=[\exp[(\varepsilon_{k\sigma}-\mu)/k_BT]+1]^{-1}$ is small, where $\varepsilon_{k\sigma}$ ($\sigma=\uparrow,\downarrow$) is the single-particle energy and μ is the chemical potential. Following conventional Boltzmann approximation, we obtain the distribution function

$$f_{k\sigma} \simeq f_0(\varepsilon_{k\sigma}) + eE\tau_{\rm el}v_{k\sigma}\frac{\partial f_0(\varepsilon_{k\sigma})}{\partial \varepsilon_{k\sigma}}, \tag{69}$$

where the electron charge is $-e$ and the spin-dependent velocity is $v_{k\sigma}\equiv\hbar^{-1}\partial\varepsilon_{k\sigma}/\partial k$. As discussed below, the spin dependence of $\varepsilon_{k\sigma}$ originates from the SU(2) gauge fields felt by the conduction electrons through the spatial modulation of the MKC. In the process of approaching to stationary

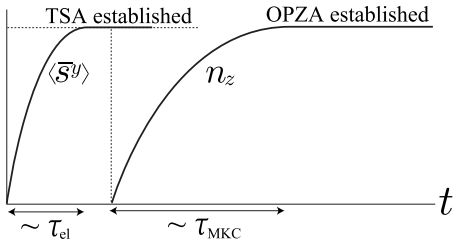

FIG. 5. The whole processes of establishing the nonadiabatic and adiabatic STTs. After switching on the electric field at $t=0$, the inequilibrium process toward the stationary flowing current state with time scale $t \simeq \tau_{\rm el}$(Boltzmann relaxation) causes the finite TSA $\langle \bar{s}_y \rangle$ and resultant nonadiabatic torque, $\mathcal{T}_2$. Then, around the time scale of $t \simeq \tau_{\rm el} + \tau_{\rm MKC}$ (Gilbert relaxation), the whole system reaches *nonequilibrium but stationary* state with the OPQZA (n_z) being established and macroscopic rotation of the DW spins being realized.

current flowing state around the time $t \sim \tau_{\rm el}$, as we will show explicitly, the statistical average of the conduction electron's spin component perpendicular to the local quantization axis, $\langle \bar{s}^y \rangle$, accumulates and acquires finite value [Fig. 3(b)]. This process is exactly the TSA. The TSA causes an additional magnetic field acting on the local moments and exert the nonadiabatic torque on the local moments. In Fig. 5, we summarize the whole processes of establishing the nonadiabatic and adiabatic STTs.

V. SLIDING CONDUCTIVITY OF THE MKC

A. General case

Plugging Eq. (69) into Eq. (67), we have

$$\mathcal{T}_2 = \gamma E. \tag{70}$$

The response coefficient γ is given by

$$\gamma = \gamma_0 \sum_{i=1}^{N_{\rm cross}} \frac{\mathcal{J}_{k_{0,i}}}{|\mathcal{J}_{k_{0,i}}|} \cosh^{-2}\left(\frac{\varepsilon_{k_{0,i}} - \mu}{2k_B T} \right), \tag{71}$$

where the quantity $\mathcal{J}_{k_{0,i}}$ defined by

$$\mathcal{J}_{k_{0,i}} \equiv v_{k_{0,i}\uparrow} - v_{k_{0,i}\downarrow} \tag{72}$$

is eligible to be called *spin current* at the band-crossing point. The special wave-number $k_{0,i}$ is determined by the condition

$$\varepsilon_{k_{0,i}\uparrow} = \varepsilon_{k_{0,i}\downarrow} \equiv \varepsilon_{k_{0,i}}. \tag{73}$$

That is to say, $k_{0,i}$ is the *band-crossing point* ($i=1,\ldots,N_{\rm cross}$ with $N_{\rm cross}$ being the number of the band-crossing points in the first Brillouin zone). It is to be noted that $k_{0,i}$ appears in the vicinity of the band extrema. So, the effect is closely related to the Van Hove singularity at which the density of states diverges. This means that the sliding conductivity is largely enhanced if the carrier density is adjustable to the Van Hove singularity. This situation may hold even for two- or three-dimensional band structure.

The factor γ_0 is given by

$$\gamma_0 = -\frac{\pi}{8}\left(\frac{L^2}{2\pi} \right)\left(\frac{J_{\rm sd} S}{k_B T} \right)\frac{e\tau_{\rm el}}{\hbar}. \tag{74}$$

Equations (51) and (70) establish relations between the terminal velocity of the MKC and the external electric field E,

$$V^* = \sigma_{\rm MKC} E, \tag{75}$$

which is the most important result in this paper. The sliding conductivity of the MKC, $\sigma_{\rm MKC}$, is given by

$$\sigma_{\rm MKC} = -\frac{\alpha^{-1} J_{\rm sd}}{\hbar q_0 L}\gamma. \tag{76}$$

In the case where only the nearest-neighbor hopping ($t_\delta = -t$) is considered, we have $k_0 = 0$ and π/a_0 to give

$$\gamma = \gamma_0 \left[\cosh^{-2}\left(\frac{\varepsilon_0 - \mu}{2k_B T} \right) - \cosh^{-2}\left(\frac{\varepsilon_0 + \mu}{2k_B T} \right) \right], \tag{77}$$

where

$$\varepsilon_0 = 2t \cos(q_0 a_0/2). \tag{78}$$

Given electron concentration per site $0 \le n \le 2$, the chemical potential μ is determined from $L^{-1}\Sigma_{k\sigma} f(\varepsilon_{k\sigma}) = n$. The dependence of $\sigma_{\rm MKC}$ on the electron concentration n is presented in Fig. 6(b). *A prominent feature is that* $\sigma_{\rm MKC}$ (i.e., *the terminal velocity* V^*) *reverses its sign depending on the free electron system is less than half filling* ($n<1$) or more than ($n>1$) *half filling. That is to say, changing the filling ratio cuases the motion reversal of the translation of the MKC in chiral helimagnet.*

By using a Drude formula for the electric current density, $j = (n_0 e^2 \tau_{\rm el}/m^*)E$ with m^* being an effective mass of carriers and n_0 being the carrier density, it is possible to make more concrete estimation of the terminal velocity and we have

$$V^* \simeq \frac{S a_0 L}{16\alpha}\left(\frac{m^*}{ne\hbar^2} \right)\left(\frac{J}{D} \right)\left(\frac{J_{\rm sd}^2}{k_B T} \right) j. \tag{79}$$

As a quantitative estimation, we take $J_{\rm sd} \simeq 1$ K$=10^{-23}$ J, $k_B T \simeq 10$ K, $\alpha \simeq 10^{-2}$, $S=1$, $D/J=10^{-1}$, $n=10^{28}$ m^{-3}, $L=10^{-2}$ m, and $a_0=10^{-10}$ m. Then, we have $V^*=10^2$ m/s for $j=10^8$ A/m^2. If the chemical potential crosses the band-crossing point, the velocity becomes resonantly huge. However, the velocity rapidly decays from $|V^*|$ upon μ deviating from the band-crossing point. So, the estimation given by Eq. (79) should be regarded as the maximum value of the terminal velocity.

Finally, we comment on the LSD, $\mathcal{S}_\parallel$. In Fig. 6(c) result of a concentration dependence for

$$\mathcal{S}_\parallel = \frac{J_{\rm sd} S L^2}{16\pi t \sin(q_0 a_0/2)} \int_{-\pi/a_0}^{\pi/a_0} dk \frac{f_{k\uparrow} - f_{k\downarrow}}{\sin k a_0} \tag{80}$$

is also shown.

B. Band splitting due to gauge field, band crossing, and motion reversal

In the case of the simplest nearest-neighbor tight-binding band, we have two crossing points $k_{0,1}=0$ and $k_{0,2}=\pi$ as

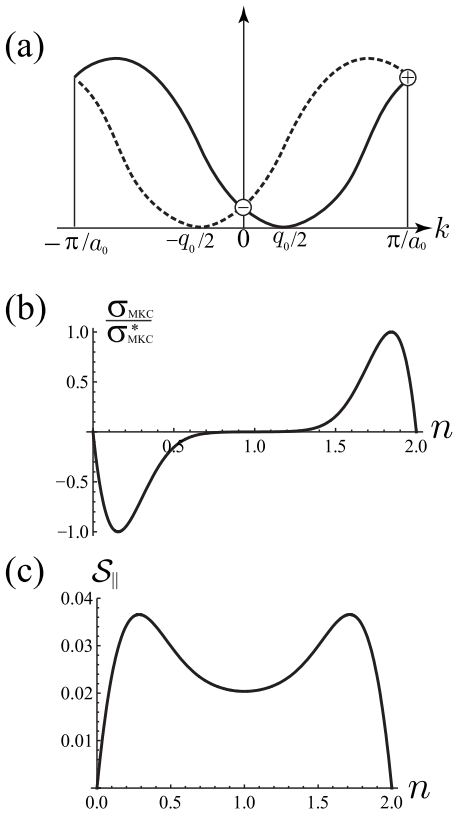

FIG. 6. (a) Band-crossings of spin-dependent bands. The crossing points are marked by circles with the sign inside them. The sign means positive or negative contributions to $\mathcal{J}_{k_{0,i}}$. (b) The sliding conductivity σ_{MKC} as a function of the carrier deinsity n. σ^*_{MKC} is the maximum value of σ_{MKC}. (c) LSD $\mathcal{S}_\parallel$ as a function of the carrier density n.

shown in Fig. 6(a). At $k_{0,1}=0$, the spin-up band has a negative slope while the spin-down bands has a positive slope and $J_{k_{0,1}}$ becomes positive. On the other hand, at $k_{0,2}=\pi$, the spin-up band has a positive slope while the spin-down bands has a negative slope and $J_{k_{0,2}}$ becomes negative. This is the direct reason why the motion reverse occurs upon changing the chemical potential μ. This mechanism of the sign reversal of the conductivity at the band-crossing points holds for general band structures.

It is to be noted that the spin up and spin down are referred to with respect to the z axis in the laboratory frame. Then, the conduction electrons see *periodic* internal gauge field (period $2\pi/q_0$) coming from the background helical magnetic structures. The band splitting is then ascribed to the difference in the phase shifts $k \to k \pm q_0/2$ acquired by the spin-up and spin-down electrons.

C. Band structure in helical crystal

Finally, we consider more realistic band structure with keeping $Cr_{1/3}NbS_2$ in mind. This crystal belongs to the space group $P6_322$. However, applied electric field violates vertical twofold rotational symmetry. Consequently, the space group 6_322 is degraded to its subgroup 6_3. In the case of Q1D, this subgroup corresponds to the line group $\underline{L}6_3$. The band structures in Q1D systems were extensively studied by Božović[38] and the case of $\underline{L}6_3$ gives the dispersion relation

$$\varepsilon_{k,\ell} = -t\cos(ka_0/2 + 2\pi\ell/6) + \varepsilon_{0,\ell},$$

where $\ell = 0, \pm 1, \pm 2, 3$ are "quasi-angular-momentum" indices. Here, a_0 is the crystallographic lattice constant. We repeat the same procedure presented before and obtained the sliding conductivity for this case. We summarize the results in Fig. 7. In this case, the band extrema occur at

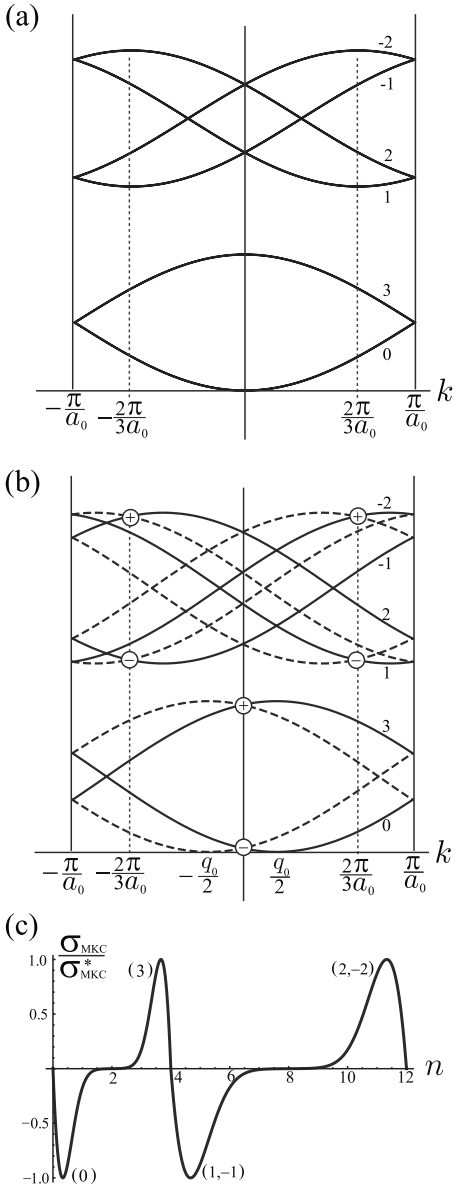

FIG. 7. (a) Symmetry-adapted energy band structure for the case of line group $\underline{L}6_3$. The quasiangular-momentum $\ell = 0, \pm 1, \pm 2, 3$ are indicated. We choose $\varepsilon_{0,0}=t$ and $\varepsilon_{0,\pm 1}=4t$. (b) Band crossings of spin-dependent bands. The crossing points are marked by circles with the sign inside them. The sign means positive or negative contributions to $\mathcal{J}_{k_{0,i}}$. (c) The sliding conductivity σ_{MKC} as a function of the carrier density n. σ^*_{MKC} is the maximum value of σ_{MKC}. Quasi-angular-momentum indices are shown for the corresponding peaks.

$k=0$, $\pm 2\pi/3a_0$, and π/a_0. Correspondingly, we have four peaks of σ_{MKC} as a function of the carrier concentration.

VI. CONCLUDING REMARKS

In this paper, we developed a consistent theory to describe the sliding motion of the MKC in terms of correlated dynamics of quantum-mechanical itinerant spins and semiclassical local moments. The most important result is given by Eqs. (75) and (76). We considered the itinerant spins as quantum-mechanical operators whereas local moments are considered within classical Lagrangian formalism. By appropriately treating fluctuations space spanned by basis functions, including a quasi-zero-mode wave function, we construct coupled equations of motion for the collective coordinate of the center-of-mass motion and the localized zero-mode coordinate perpendicular to the domain-wall plane. By solving them, we demonstrate that the correlated dynamics is understood through a hierarchy of two time scales: Boltzmann relaxation time τ_{el}, when a nonadiabatic part of the spin-transfer torque, $\mathcal{T}_2$, appears, and Gilbert damping time τ_{MKC}, when adiabatic part, $\mathcal{T}_1$, comes up.

Now, the appearance of the nonadiabatic spin-transfer-torque is understood as follows. Once the electric field is switched on, electrons rapidly travel over the MKC and relax to the stationary state after the Boltzmann relaxation time τ_{el}. During this process, they cannot instantly follow the background MKC. This mistracking causes the TSA of the itinerant spin along the local $\bar{y}$ axis, $\langle \bar{s}^{\bar{y}} \rangle$. Appearance of this off-diagonal expectation value is justified by the spin-flipping process caused by the sd interaction. The TSA creates the nonadiabatic torque, $\mathcal{T}_2$, on the local moments. Microscopically, the background MKC causes gauge field acting on the itinerant spins and lifts the degeneracy between spin-up and spin-down bands. Because of this band splitting, the spin current $\mathcal{J}_{k_0}$ naturally comes up and gives rise to stationary torque on the local moments.

Once the TSA is established, the local spins rotate around the local $\bar{y}$ axis by the nonadiabatic torque and finally relax to a new stationary state after the time scale of the Gilbert relaxation of the MKC state, τ_{MKC}. Then, the out-of-plane (z) component of the local moments accumulates. This accumulation is referred to as OPQZA which causes the adiabatic torque, $\mathcal{T}_1$, (Döring mechanism[13]) on the local moments and leads to the stationary motion of the whole MKC. Because of this mechanism, the sliding motion of the MKC accompanies the transport magnetic current, which is detectable in experiments.[21]

As for candidate to test our prediction, the metallic chiral helimagnet $Cr_{1/3}NbS_2$ (Refs. 27 and 28) may be promising, because this material contains itinerant and localized species of spins, respectively, coming from the partially filled d subband of Nb and the filled d levels of Cr^{3+} giving local spin $S=5/2$. Metallic chiral helimagnet MnSi may also be an eligible candidate. To make more plausible connection between the present theory and experiments, details of the interaction between localized and itinerant species of spins should be clarified. A guiding principle for materializing this effect is symmetry-adapted material synthesis (as exemplified in Sec. V C), because the chiral helimagnetic structure is stabilized only in materials without rotoinversion symmetry, i.e., the interplay of crystallographic and magnetic chirality plays a key role there. We hope our finding opens a new field of spintronics based on the crystal structure engineering.

ACKNOWLEDGMENTS

J.-i.K. acknowledges Grant-in-Aid for Scientific Research (C) (Grant No. 19540371) from the Ministry of Education, Culture, Sports, Science and Technology, Japan. A.S.O. and I.V.P. acknowledge RFBR under Grant No. 10-02-00098-a.

[1] J. C. Slonczewski, J. Magn. Magn. Mater. **159**, L1 (1996).
[2] L. Berger, J. Appl. Phys. **49**, 2156 (1978).
[3] L. Berger, Phys. Rev. B **54**, 9353 (1996).
[4] M. D. Stiles and A. Zangwill, Phys. Rev. B **66**, 014407 (2002).
[5] S. Zhang, P. M. Levy, and A. Fert, Phys. Rev. Lett. **88**, 236601 (2002).
[6] Ya. B. Bazaliy, B. A. Jones, and S.-C. Zhang, Phys. Rev. B **57**, R3213 (1998).
[7] G. Tatara and H. Kohno, Phys. Rev. Lett. **92**, 086601 (2004).
[8] G. Tatara, H. Kohno, and J. Shibata, Phys. Rep. **468**, 213 (2008).
[9] A. Thiaville, Y. Nakatani, J. Miltat, and Y. Suzuki, Europhys. Lett. **69**, 990 (2005).
[10] S. Zhang and Z. Li, Phys. Rev. Lett. **93**, 127204 (2004).
[11] J. Xiao, A. Zangwill, and M. D. Stiles, Phys. Rev. B **73**, 054428 (2006).
[12] J. I. Kishine and A. S. Ovchinnikov, Phys. Rev. B **81**, 134405 (2010).
[13] W. Döring, Z. Naturforsch. B **3a**, 374 (1948); R. Becker, Proceedings of the Grenoble Conference, July, 1950 (unpublished); C. Kittel, Phys. Rev. **80**, 918 (1950).
[14] J. He, Z. Li, and S. Zhang, Phys. Rev. B **73**, 184408 (2006).
[15] O. Wessely, B. Skubic, and L. Nordström, Phys. Rev. Lett. **96**, 256601 (2006).
[16] O. Wessely, B. Skubic, and L. Nordström, Phys. Rev. B **79**, 104433 (2009).
[17] S. Mühlbauer, B. Binz, F. Jonietz, C. Pfleiderer, A. Rosch, A. Neubauer, R. Georgii, P. Böni, Science **323**, 915 (2009).
[18] I. E. Dzyaloshinsky, J. Phys. Chem. Solids **4**, 241 (1958)
[19] I. E. Dzyaloshinskii, Sov. Phys. JETP **19**, 960 (1964); **20**, 665 (1965).
[20] Yu. A. Izyumov, Sov. Phys. Usp. **27**, 845 (1984).
[21] I. G. Bostrem, J. I. Kishine, and A. S. Ovchinnikov, Phys. Rev. B **77**, 132405 (2008); **78**, 064425 (2008).
[22] A. B. Borisov, J. I. Kishine, I. G. Bostrem, and A. S. Ovchinnikov, Phys. Rev. B **79**, 134436 (2009).
[23] J. I. Kishine and A. S. Ovchinnikov, Phys. Rev. B **79**, 220405(R) (2009).
[24] J. Kishine, K. Inoue, and Y. Yoshida, Prog. Theor. Phys. **159**, 82

(2005).

[25] When the local spins couple with itinerant spins, it is natural to expect long-range spin-spin interaction of the Ruderman-Kittel-Kasuya-Yoshida type arises. In this case, the symmetric exchange interaction term includes higher even-order derivatives of $\mathbf{n}$ such as $\partial^4\mathbf{n}/\partial z^4$ and the DM term includes odd-order ones such as $\partial^3\mathbf{n}/\partial z^3$. However, as far as we consider $\mathbf{n}$ as slowly varying function, it may be qualitatively enough to retain only the lowest order derivatives.

[26] L. L. Liu, Phys. Rev. Lett. **31**, 459 (1973).

[27] T. Moriya and T. Miyadai, Solid State Commun. **42**, 209 (1982); T. Miyadai, K. Kikuchi, H. Kondo, S. Sakka, M. Arai, and Y. Ishikawa, J. Phys. Soc. Jpn. **52**, 1394 (1983).

[28] Y. Kousaka, Ph.D. thesis, Aoyama-gakuin University, 2009.

[29] B. Sutherland, Phys. Rev. A **8**, 2514 (1973).

[30] I. G. Bostrem, J. Kishine, R. V. Lavrov, and A. S. Ovchinnikov, Phys. Lett. A **373**, 558 (2009).

[31] R. Rajaraman, *Solitons and Instantons: An Introduction to Solitons and Instantons in Quantum Field Theory* (North-Holland, Amsterdam, New York, 1982).

[32] In the case of a single DW problem, the energy gap of the out-of-plane mode originates from the hard-axis anisotropy energy (see Ref. 12). In the chiral helimagnet, the DM interaction plays a role of the hard-axis anisotropy. Furthermore, the zero/quasizero mode in the MKC state appears at the bottom of *continuous* bands. This situation is in contrast to the DW problem, where these modes appear as localized modes isolated from the spin-wave modes.

[33] G. C. Cabrera and L. M. Falikov, Phys. Status Solidi B **61**, 539 (1974).

[34] V. Korenman, J. L. Murray, and R. E. Prange, Phys. Rev. B **16**, 4032 (1977).

[35] G. Tatara and H. Fukuyama, J. Phys. Soc. Jpn. **63**, 2538 (1994).

[36] L. V. Keldysh, Sov. Phys. JETP **20**, 1018 (1965).

[37] C. Niu, D. L. Lin, and T.-H. Lin, J. Phys.: Condens. Matter **11**, 1511 (1999).

[38] I. Božović, Phys. Rev. B **29**, 6586 (1984).